Available online at www.sciencedirect.com
ScienceDirect
Ceramics International 37 (2011) 2159–2164
CERAMICS INTERNATIONAL
www.elsevier.com/locate/ceramint

Properties and rapid consolidation of nanostructured Al_2O_3-Al_2SiO_5 composites by high frequency induction heated sintering

In-Jin Shon [a,*], In-Yong Ko [a], Hyun-Su Kang [a], Kyung-Tae Hong [b], Jung-Mann Doh [b], Jin-Kook Yoon [b]

[a] *Division of Advanced Materials Engineering and the Research Center of Advanced Materials Development, Engineering College, Chonbuk National University, 561-756, Republic of Korea*
[b] *Advanced Functional Materials Research Center, Korea Institute of Science and Technology, PO Box 131, Cheongryang, Seoul 130-650, Republic of Korea*

Received 26 November 2010; received in revised form 18 January 2011; accepted 2 March 2011
Available online 8 April 2011

Abstract

The rapid sintering of nanostructured Al_2O_3 and Al_2O_3 to Al_2SiO_5 composites was investigated by a high-frequency induction heating sintering process. The advantage of this process is that it allows very quick densification to near theoretical density and inhibition of grain growth. Highly dense nanostructured Al_2O_3 and Al_2O_3 to Al_2SiO_5 composites were produced with simultaneous application of a 80 MPa pressure and induced output current of a total power capacity (15 kW) within 3 min. The sintering behavior, grain size and mechanical properties of Al_2O_3 and Al_2O_3 to Al_2SiO_5 composites were investigated.

Keywords: Sintering; Al_2O_3; Al_2SiO_5; Nanostructured material; Powder metallurgy

1. Introduction

Al_2SiO_5 has achieved outstanding importance as a material for both traditional and advanced ceramics because of its high thermal stability and favorable properties such as low thermal expansion and conductivity, high creep resistance and corrosion stability [1]. However, as in the cases of many ceramic materials, there are concerns regarding low fracture toughness below the ductile-brittle transition temperature. To improve their mechanical properties, the common approach has been the addition of a second phase to form composites and make nanostructured materials. One example is the addition of Al_2O_3 to Al_2SiO_5 to improve the properties. The attractive properties of Al_2O_3 are high hardness, low density (3.97 g/cm^3), good biocompatibility and good oxidation resistance [2,3].

Nanocrystalline materials have received much attention as advanced engineering materials with improved physical and mechanical properties [4,5]. More attention has been paid to the applications of nanomaterials that take advantage of their high strength, hardness, excellent ductility and toughness [6,7]. Recently, nanocrystalline powders have been developed by thermochemical and thermomechanical spray conversion process (SCP), co-precipitation and high-energy milling [8–10]. However, the grain size in sintered materials becomes much larger than that in pre-sintered powders due to fast grain growth during the conventional sintering process. Therefore, even though the initial particle size is less than 100 nm, the grain size increases rapidly up to 2 μm or larger during the conventional sintering [11]. Therefore, controlling grain growth during sintering is key to the commercial success of nanostructured materials. As a result, the high frequency induction heated sintering method (HFIHS), which can fabricate dense materials within 2 min, has been shown to be effective in achieving this goal [12–15].

In this work, we investigated the sintering of Al_2O_3-Al_2SiO_5 composites by the HFIHS method. The goal of this research is to produce dense nanostructured Al_2O_3-Al_2SiO_5 hard materials. In addition, we also studied the effect of Al_2O_3 on mechanical properties of Al_2O_3-Al_2SiO_5 composites.

* Corresponding author. Tel.: +82 63 2381; fax: +82 63 270 2386.
E-mail address: ijshon@chonbuk.ac.kr (I.-J. Shon).

0272-8842/$36.00
doi:10.1016/j.ceramint.2011.03.060

2. Experimental procedures

Al_2O_3 powder with an average grain size <2.2 μm with 99.99% purity and amorphous SiO_2 powder with a grain size <1 μm with purity were supplied by Alfa. The powders (Al_2O_3, Al_2O_3-10wt%SiO_2, Al_2O_3-20wt%SiO_2, Al_2O_3-30wt%SiO_2, Al_2O_3-40wt%SiO_2, Al_2O_3-50wt%SiO_2) were first milled in a high-energy ball mill (Pulverisette-5 planetary mill) at 250 rpm for 4 h. Tungsten carbide balls (9 mm in diameter) were used in a sealed cylindrical stainless steel vial under an argon atmosphere. The weight ratio of balls-to-powder was 30:1. Milling resulted in significant reductions of the grain size. The grain sizes of the Al_2O_3 and Al_2SiO_5 were calculated from the full width at half-maximum (FWHM) of the diffraction peak using Suryanarayana's and Grant Norton's formula [16]:

$$Br(\mathrm{Bcrystalline} + \mathrm{Bstrain})\cos\theta = k\lambda/L + \eta\sin\theta \quad (1)$$

where B_r is the FWHM of the diffraction peak after instrument correction; $B_{crystalline}$ and B_{strain} are the FWHM caused by a small grain size and internal stress, respectively; k is a constant with a value of 0.9; λ is the wavelength of the X-ray radiation; L and η are the grain size and internal strain, respectively; and θ is the Bragg angle. The parameters B and Br follow Cauchy's form with the relationship: $B = B_r + B_s$, where B and B_s are the FWHM of the broadened Bragg peaks and the standard sample's Bragg peaks, respectively.

The powders were placed in a graphite die (outside diameter, 45 mm; inside diameter, 20 mm; height, 40 mm) and then introduced into the HFIHS apparatus described [12–15]. The HFIHS apparatus includes a 15 kW power supply that provides an induced current through the sample and a 50 kN uniaxial press. The system was first evacuated and a uniaxial pressure of 80 MPa was applied. An induced current was then activated and maintained until the densification rate was negligible, as indicated by real-time output of the sample shrinkage. The shrinkage was measured by a linear gauge measuring the vertical displacement. The HFIHS can be controlled in two ways: temperature and output. The latter was chosen to investigate the effect of the total power output given that the induced current level has a direct effect on the rate of heating and maximum temperature. The output level was 80% of the total power output. Temperatures were measured by a pyrometer focused on the surface of the graphite die. At the end of the process, the induced current was turned off and the sample was cooled to room temperature. The process was performed under a vacuum of 5.33 Pa.

The relative density of the sintered sample was measured by the Archimedes method. Microstructural information was obtained from product samples, which had been polished and etched using thermal etching for 1 h at 1100°C. Compositional and microstructural analyses of the products were performed via X-ray diffraction (XRD) and field emission scanning electron microscopy (FE-SEM) with energy dispersive spectroscopy (EDS). Vickers hardness was measured by performing indentations at a load of 5 kg and a dwell time of 15 s.

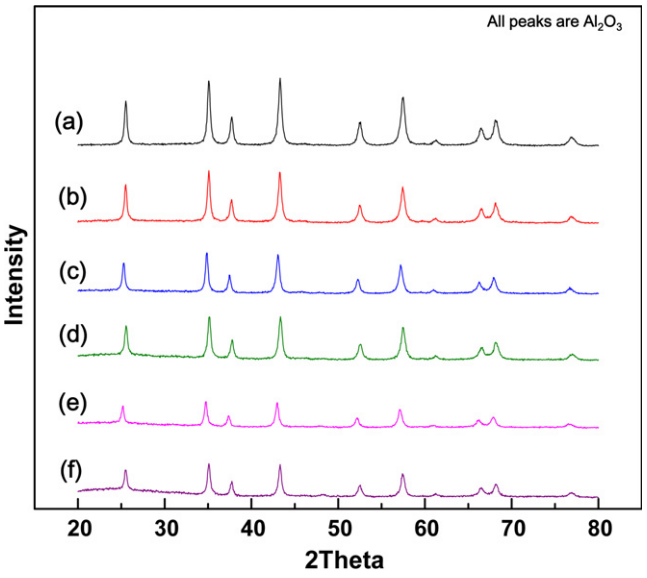

Fig. 1. X-ray diffraction patterns of powder milled for 4 h; (a) Al_2O_3, (b) Al_2O_3-10wt%SiO_2, (c) Al_2O_3-20wt%SiO_2, (d) Al_2O_3-30wt%SiO_2 and (e) Al_2O_3-40wt%SiO_2 (f) Al_2O_3-50wt%SiO_2.

3. Results and discussion

Fig. 1 shows the XRD patterns of the Al_2O_3, Al_2O_3-10wt%SiO_2, Al_2O_3-20wt%SiO_2, Al_2O_3-30wt%SiO_2, Al_2O_3-40wt%SiO_2, and Al_2O_3-50wt%SiO_2 powders after high-energy ball milling for 4 h. Only Al_2O_3 peaks were detected and SiO_2 peaks were not detected due to amorphous phase. Fig. 2 shows plot of Brcosθ versus sinθ of Al_2O_3 milled for 4 h to calculate particle size from XRD data. The average grain size of the Al_2O_3 as determined by Suryanarayana's and Grant Norton's formula was approximately 40 nm.

FE-SEM images of Al_2O_3, Al_2O_3-10wt%SiO_2, Al_2O_3-20wt%SiO_2, Al_2O_3-30wt%SiO_2, Al_2O_3-40wt%SiO_2, and Al_2O_3-50wt%SiO_2 powder with milling for 4 h are shown in Fig. 3. Al_2O_3 and SiO_2 powders were round, refined by milling and agglomerated. The shrinkage displacement and tempera-

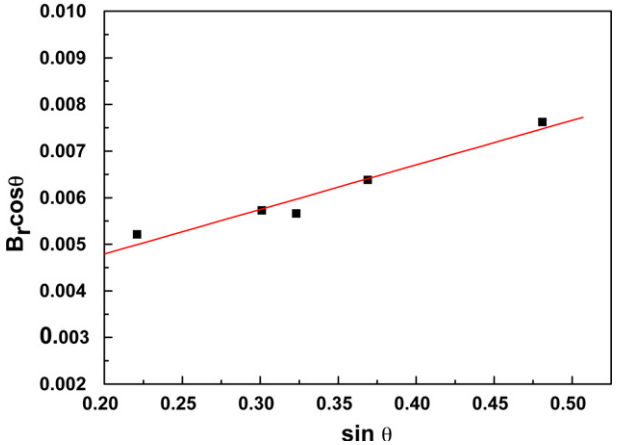

Fig. 2. Plot of B_r ($B_{crystalline}$ + B_{strain}) cosθ versus sinθ for Al_2O_3 powder milled for 4 h.

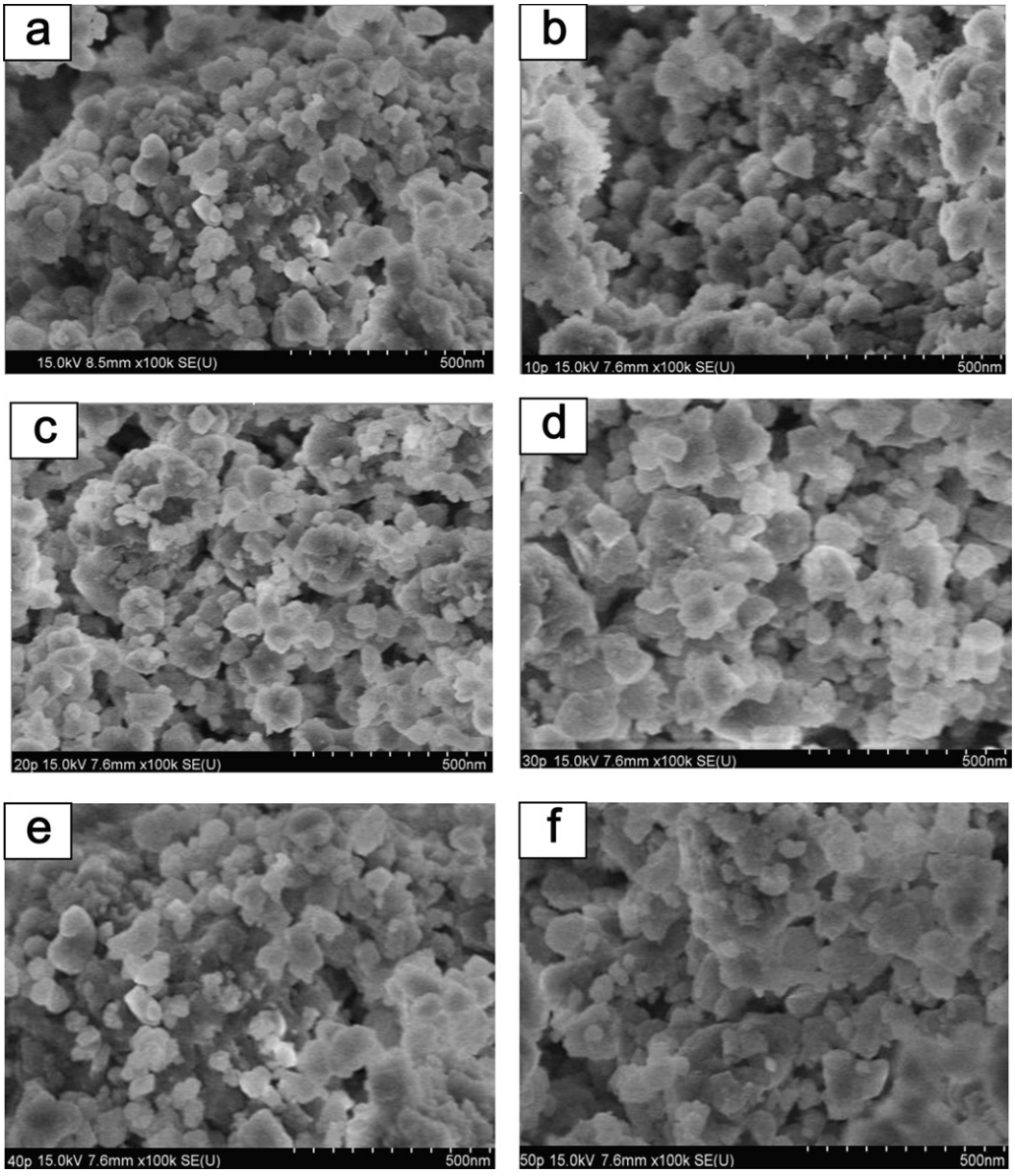

Fig. 3. FE-SEM images of powder milled for 4 h; (a) Al_2O_3, (b) Al_2O_3-10wt%SiO_2, (c) Al_2O_3-20wt%SiO_2, (d) Al_2O_3-30wt%SiO_2, and (e) Al_2O_3-40wt%SiO_2, (f) Al_2O_3-50wt%SiO_2.

ture according to heating time for 80% of the total output power capacity (15 kW) during the sintering of high-energy ball milled Al_2O_3, Al_2O_3-10wt%SiO_2, Al_2O_3-20wt%SiO_2, Al_2O_3-30wt%SiO_2, Al_2O_3-40wt%SiO_2, and Al_2O_3-50wt%SiO_2 powders under a pressure of 80 MPa are shown in Fig. 4. In all cases, the application of induced current resulted in shrinkage due to consolidation. As induced current was applied, all specimens exhibited thermal expansion and the shrinkage initiation abruptly increased. The temperature varied from 1070 to 1220 K depending on the milling time. The temperature at which shrinkage started decreased with increasing milling time, and the high-energy ball milling affected the rate of densification and the final density. High-energy ball milling treatment allows control of compound formation by fixing the Al_2O_3 powder microstructure. Indeed, high-energy ball milling produces finer crystallites, strain and defects. Therefore, the consolidation temperature decreases with milling time because the driving forces for sintering and contact points of powders for atomic diffusion increase. Fig. 5 shows the XRD patterns of specimens sintered from the high-energy ball milled Al_2O_3, Al_2O_3-10wt%SiO_2, Al_2O_3-20wt%SiO_2, Al_2O_3-30wt%SiO_2, Al_2O_3-40wt%SiO_2, and Al_2O_3-50wt%SiO_2 powders, in which all the peaks in Fig. 5(a) were Al_2O_3. Al_2O_3 and $Al2SiO_5$ peaks were detected in the Al_2O_3-SiO_2 system. The interaction between these phases, i.e.,

$$Al_2O_3 + SiO_2 \rightarrow Al_2SiO_5 \quad (2)$$

was thermodynamically feasible [17].

The plot of B_r ($B_{crystalline} + B_{strain}$) cosθ versus sinθ in Suryanarayana's and Grant Norton's formula [16] is shown in Fig. 7 The average grain sizes of Al_2O_3 and Al_2SiO_5 in Al_2O_3, Al_2O_3-10wt%SiO_2, Al_2O_3-20wt%SiO_2, Al_2O_3-30wt%SiO_2,

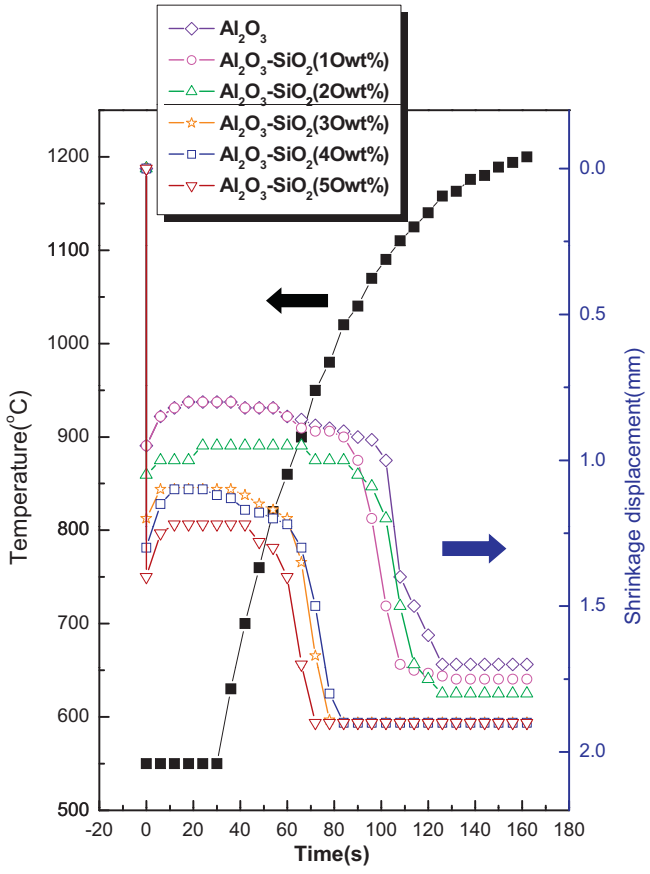

Fig. 4. Temperature and shrinkage according to heating time during the sintering of Al_2O_3-SiO_2 powders milled for 4 h.

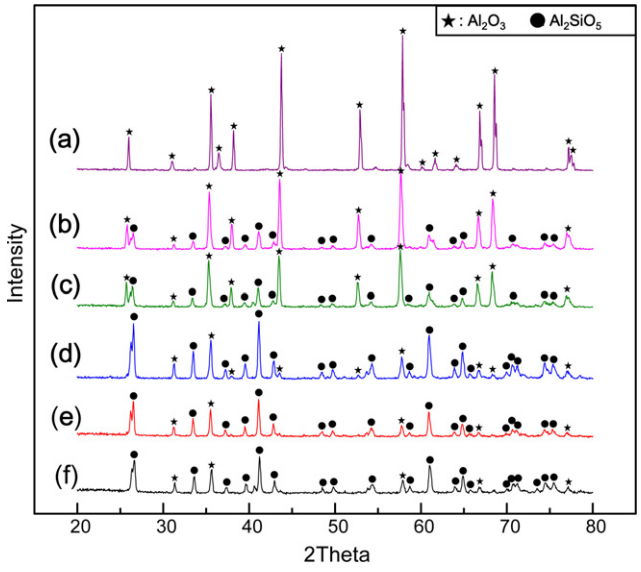

Fig. 5. X-ray diffraction patterns of sintered specimens; (a) Al_2O_3, (b) Al_2O_3-10wt%SiO_2, (c) Al_2O_3-20wt%SiO_2, (d) Al_2O_3-30wt%SiO_2, and (e) Al_2O_3-40wt%SiO_2, (f) Al_2O_3-50wt%SiO_2.

Al_2O_3-40wt%SiO_2, and Al_2O_3-50wt%SiO_2 systems calculated from the XRD data using Suryanarayana's and Grant Norton's formula [16] were approximately 80, 101, 148, 140, 96, 143 nm and 56, 75, 121, 96, 29 nm, respectively. The relative density of Al_2O_3 sintered from milled Al_2O_3 powder was 99%. Thus, the average grain size of the sintered Al_2O_3 and Al_2SiO_5 was not much larger than that of the initial powder, indicating the absence of significant grain growth during sintering. This retention of grain size was attributed to the fast heating rate and relatively short-term exposure of the powders to the high temperature. As the initial particle size of the Al_2O_3 powder increased, the porosity also increased. The SEM images of Al_2O_3 sintered from powder milled for various times are shown in Fig. 8 The fine pores of the Al_2O_3 sample decreased with increasing milling time. Fig. 8 shows SEM images of Al_2O_3 sintered from various milled powders. From the figures, the grain boundary is not clear but the average grain size seems to be several microns. FE-SEM images of Al_2O_3 and Al_2O_3-Al_2SiO_5 sintered from Al_2O_3, Al_2O_3-10wt%SiO_2, Al_2O_3-20wt%SiO_2, Al_2O_3-30wt%SiO_2, Al_2O_3-40wt%SiO_2, and Al_2O_3-50wt%SiO_2 powders milled for 4 h are shown in Fig. 6. Al_2O_3 and Al_2SiO_5 consist of nanocrystals. The differences in average grain size detected by SEM images and XRD data were due to the nanocrystalline Al_2O_3 grains.

The role of current (resistive or inductive) in sintering or synthesis has been the focus of several studies aimed at explaining enhanced sintering and improved product characteristics. The role played by current has been interpreted in terms of the fast heating rate due to Joule heating, the presence of plasma in pores separating powder particles [18], and the intrinsic contribution of the current to mass transport [19–21].

Vickers hardness measurements were performed on polished sections of Al_2O_3 and Al_2O_3-Al_2SiO_5 samples using a 5 kg load and 15 s dwell time. The Vickers hardnesses of Al_2O_3 and Al_2O_3-Al_2SiO_5 sintered from Al_2O_3, Al_2O_3-10wt%SiO_2, Al_2O_3-20wt%SiO_2, Al_2O_3-30wt%SiO_2, Al_2O_3-40wt%SiO_2, and Al_2O_3-50wt%SiO_2 powders milled for 4 h the Al_2O_3 were 1820, 1681, 1319, 1132, 1049 and 941 kg/mm^2, respectively. The hardnesses of Al_2O_3-Al_2SiO_5 composites increased with an increase in Al_2O_3 content.

Indentations with sufficient loads produced median cracks near each indent. The lengths of these cracks permits the estimation of the fracture toughness of the materials by the following equation [22]:

$$K_{IC} = 0.204(c/a)^{-3/2} \cdot H_v \cdot a^{1/2} \quad (3)$$

where c is the trace length of the crack measured from the center of the indentation, a is one half of the average lengths of the two indent diagonals, and H_v is the hardness. The calculated fracture toughness values for the Al_2O_3-Al_2SiO_5 composites sintered from Al_2O_3-10wt%SiO_2, Al_2O_3-20wt%SiO_2, Al_2O_3-30wt%SiO_2, Al_2O_3-40wt%SiO_2, and Al_2O_3-50wt%SiO_2 powders were approximately 5, 6, 4.3, 3, 3 and 3 MPa·m$^{1/2}$, respectively. As for the hardness values, the final toughness values were the averages of five measurements each. The fracture toughnesses of Al_2O_3-Al_2SiO_5 composites increased with increases in Al_2O_3 content because the fracture toughness of Al_2O_3 is greater than Al_2SiO_5 [1].

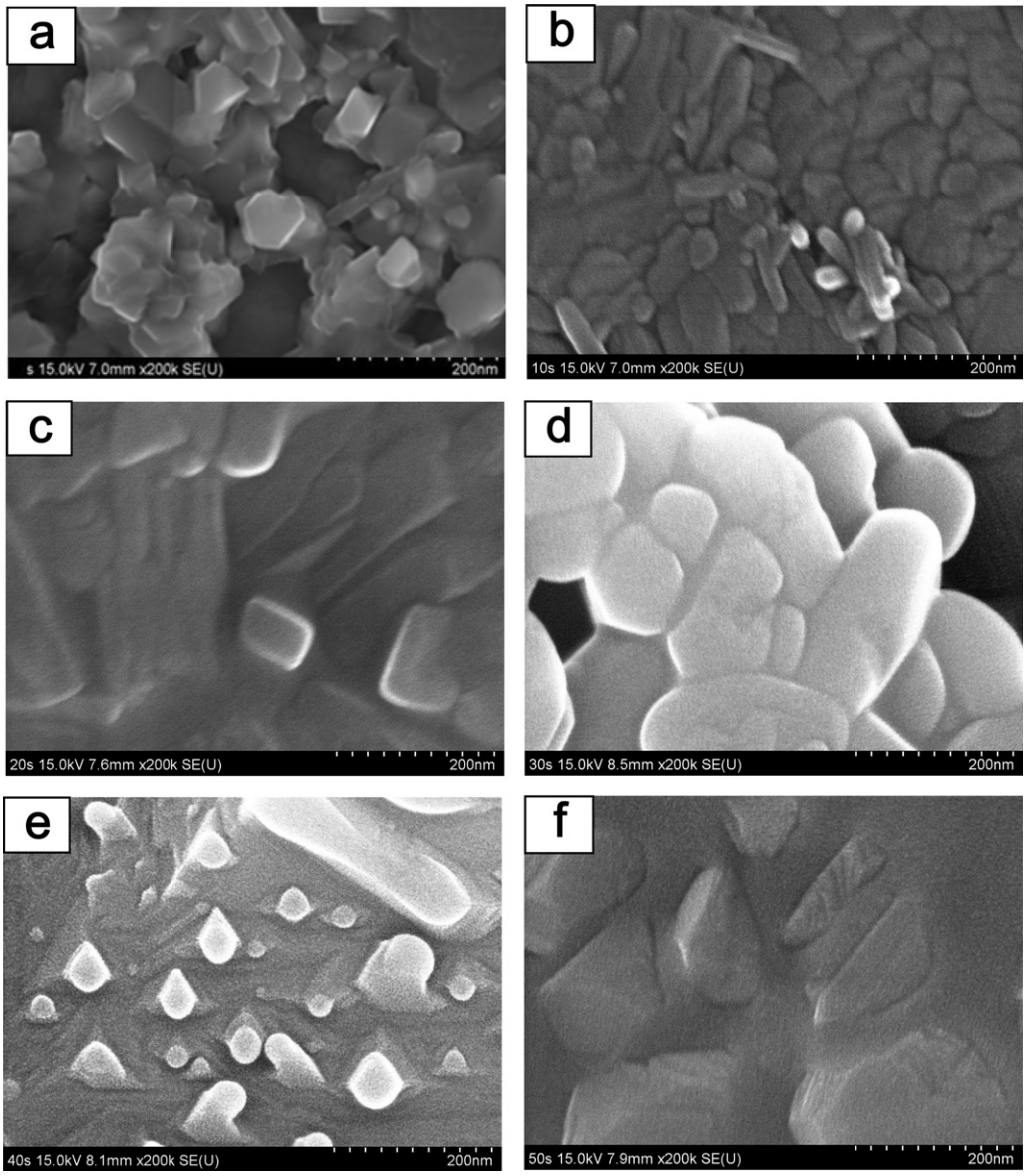

Fig. 6. FE-SEM image of sintered specimens: (a) Al_2O_3, (b) Al_2O_3-10wt%SiO_2, (c) Al_2O_3-20wt%SiO_2, (d) Al_2O_3-30wt%SiO_2, and (e) Al_2O_3-40wt%SiO_2, (f) Al_2O_3-50wt%SiO_2.

4. Summary

Using a new rapid sintering method, HFIHS, the densification of Al_2O_3 and Al_2O_3-Al_2SiO_5 was accomplished using high-energy ball milling. The average grain sizes of the Al_2O_3 and Al_2SiO_5 in Al_2O_3, Al_2O_3-10wt%SiO_2, Al_2O_3-20wt%SiO_2, Al_2O_3-30wt%SiO_2, Al_2O_3-40wt%SiO_2, and Al_2O_3-50wt%SiO_2 systems were approximately 80, 101, 148, 140, 96, 143 nm and 56, 75, 121, 96, 29 nm, respectively. The relative density of Al_2O_3 sintered from the milled Al_2O_3 powder was 99%. The Vickers hardnesses of Al_2O_3 and Al_2O_3-Al_2SiO_5 sintered from Al_2O_3, Al_2O_3-10wt%SiO_2, Al_2O_3-20wt%SiO_2, Al_2O_3-30wt%SiO_2, Al_2O_3-40wt%SiO_2, and Al_2O_3-50wt%SiO_2 powders milled for 4 h were 1820, 1681, 1319, 1132, 1049 and 941 kg/mm^2, respectively. The hardnesses of Al_2O_3-Al_2SiO_5 composites increased with increases in Al_2O_3 content. The fracture toughnesses of Al_2O_3-Al_2SiO_5 composites increased with increasees in Al_2O_3 content because the fracture toughness of Al_2O_3 is greater than that of Al_2SiO_5

Acknowledgments

We are grateful for financial support from the Korea Institute of Science and Technology, which was provided through the Program for Study on Development of Surface Treatment for Light Metals.

References

[1] H. Schneider, J. Schreuer, B. Hildmann, structure and properties of mullite-a review, Journal of the EUROPEAN Ceramic Society 28 (2008) 329–344.

[2] M.N. Rahaman, A.Y. Yao, B.S. Bal, J.P. Garino, M.D. Ries, Ceramics for prosthetic hip and joint replacement, J. Am. Ceram. Soc 90 (7) (2007) 1965–1988.
[3] W. Gao, Z. Li, D. Zhang, A new high-temperature, oxidation-resistant Ti-based material, Oxidation of Metals 57 (1/2) (2002) 99–114.
[4] M. Sherif El-Eskandarany, Structure and properties of nanocrystalline TiC full-density bulk alloy consolidation from mechanically reacted powders, J. Alloys & Compounds 305 (2000) 225–238.
[5] L. Fu, L.H. Cao, Y.S. Fan, Two-step synthesis of nanostuctured tungsten carbide-cobalt powders, Scripta Materialia 44 (2001) 1061–1068.
[6] K. Niihara, A. Nikahira, Advanced structural Inorganic Composite, Elsevier Scientific Publishing Co., Trieste, Italy, 1990.
[7] S. Berger, R. Porat, R. Rosen, Nanocrystalline materials: A study of WC-based hard metals, Progress in Materials 42 (1997) 311–320.
[8] Z. Fang, J.W. Eason, Study of nanostuctured WC-Co composites, Int. J. of Refractory Met. & Hard Mater 13 (1995) 297–303.
[9] A.I.Y. Tok, L.H. Luo, F.Y.C. Boey, Carbonate Co-precipitation of Gd_2O_3-doped CeO_2 solid solution nano-particles, Materials Science and Engineering A 383 (2004) 229–234.
[10] I.J. Shon, D.K. Kim, I.Y. Ko, J.K. Yoon, K.T. Hong, Fabrication of nanocrystalline $TaSi_2$ composite by high frequency induction heated combustion synthesis and its mechanical properties, Materials Science Forum 534–536 (2007) 525–528.
[11] J. Jung, S. Kang, Sintered (Ti,W)C carbides, Scripta Materialia 56 (2007) 561–564.
[12] H.C. Kim, D.Y. Oh, J. Guojian, I.J. Shon, Synthesis of WC and dense WC-5vol%Co hard materials by high-frequency induction heated combustion, Mater. Sci. Eng. A 368 (2004) 10–17.
[13] H.C. Kim, D.Y. Oh, I.J. Shon, Sintering of nanophase WC-15vol.%Co hard matals by rapid sintering process, Int. J. Refract. Metals & Hard Mater. 22 (2004) 197–203.
[14] D.Y. Oh, H.C. Kim, J.K. Yoon, I.J. Shon, Simultaneous synthesis and consolidation process of ultra-fine WSi_2–SiC and its mechanical properties, J. Alloys & Compounds 386 (2005) 270–275.
[15] H.C. Kim, D.Y. Oh, I.J. Shon, Synthesis of WC and dense WC-xvol.%Co hard materials by high-frequnecy induction heated combustion method, Int. J. Refract. Metals & Hard Mater 22 (2004) 41–49.
[16] C. Suryanarayana, M. Grant Norton, X-ray Diffraction A Practical Approach, Plenum Press, New York, 1998.
[17] O. Knacke, O. Kubaschewski, K. Hesselmann, Thermo chemical Properties of Inorganic Substances, Springer-Verlag, 1991.
[18] Z. Shen, M. Johnsson, Z. Zhao, M. Nygren, Spark plasma sintering of alumina, J. Am. Ceram. Soc 85 (2002) 1921–1927.
[19] J.E. Garay, U. Anselmi-Tamburini, Z.A. Munir, S.C. Glade, P. Asoka-Kumar, Electric Current Enhanced Defect Mobility in Ni_3Ti Intermetallics, Appl. Phys. Lett 85 (2004) 573–575.
[20] J.R. Friedman, J.E. Garay, U. Anselmi-Tamburini, Z.A. Munir, Modified interfacial reactions in Ag–Zn multilayers under the influence of high DC currents, Intermetallics 12 (2004) 589–597.
[21] J.E. Garay, J.E. Garay, U. Anselmi-Tamburini, Z.A. Munir, Enhanced growth of intermetallic phases in the Ni–Ti system by current effects, Acta Mater. 51 (2003) 4487–4495.
[22] K. Niihara, R. Morena, D.P.H. Hasselman, Evaluation of KIC of Brittle Solids by the Indentation Method with Low Crack-to-Indent Ratios, J. Mater. Sci. Lett. 1 (1982) 12–16.